Electrochimica Acta 308 (2019) 277–284

Contents lists available at ScienceDirect

Electrochimica Acta

journal homepage: www.elsevier.com/locate/electacta

Investigating electron transport in a PEDOT/Quinone conducting redox polymer with in situ methods

Mia Sterby [a], Rikard Emanuelsson [a], Fikret Mamedov [b], Maria Strømme [a], Martin Sjödin [a, *]

[a] Nanotechnology and Functional Materials, Department of Engineering Sciences, The Ångström Laboratory, Uppsala University, Box 534, SE-751 21, Uppsala, Sweden
[b] Molecular Biomimetics, Department of Chemistry - Ångström, The Ångström Laboratory, Uppsala University, Box 523, SE-751 20, Uppsala, Sweden

ARTICLE INFO

Article history:
Received 18 January 2019
Received in revised form
29 March 2019
Accepted 30 March 2019
Available online 2 April 2019

ABSTRACT

A conducting redox polymer is investigated in acidic electrolyte using various in situ methods, including electron paramagnetic resonance (EPR), UV–vis spectroscopy, and conductance measurements. The quinone redox active pendant group has a formal potential of 0.67 V (vs. standard hydrogen electrode) where a 2e2H process occurs. By analyzing the rate constant at different temperatures, the rate-limiting step in the redox reaction was found to be a thermally activated process with an activation energy of 0.3 eV. The electron transport through the conducting polymer was found to be non-thermally activated and, hence, not redox rate-limiting. This is also the first time a negative temperature dependence has been reported for a conducting redox polymer in the same potential region where the redox active pendant group has its formal potential. EPR and conductance data indicated that the conductivity is governed by both polarons and bipolarons but their ratio is shifting during oxidation and reduction of the polymer.

1. Introduction

There is an increased demand for electrical energy storage (EES) in order to be able to store energy harvested from sustainable sources such as wind, waves, or the sun and to power all the portable devices being used in the modern world [1]. But at the same time climate change is forcing us to reconsider what materials and methods we are using to produce such EES devices. Future EES devices need to have a sustainable life cycle from the acquiring of raw materials to the recycling and disposal processes. Organic batteries have the possibility to be more environmentally friendly than their inorganic counterparts since they can be made from renewable resources and do not require energy consuming mining and refining as metal-based batteries do [2]. With organic materials, the electronic properties can also be fine-tuned to fit different applications and they can be made flexible [3,4]. Organic battery materials can be categorized by several different means, e.g. by the nature of the redox active group (radical [5,6], carbonyl group [4,7,8], conjugated polymer [9,10], etc.), by the size of the molecular building block, or in a more traditional way, by the cycling ion (H^+ [11,12], Li^+ [13,14], Na^+ [7,15], etc.). A particular class in the family of organic battery materials that has recently gained attention is conducting redox polymers [11,16–18]. These materials contain both a conjugated polymer and a small redox active functional group. The principal design serves to combine the strengths of the large polymeric system with the electronic properties of conjugated polymers and other specific redox groups. Conjugated polymers are electrically conducting and insoluble but suffer from low charge storage capacity and a poorly defined redox potential. Small redox groups on the other hand have a high charge storage capacity and, in many cases, a well-defined redox potential but can dissolve in the electrolyte and are not conducting. By covalently attaching small redox groups to the conducting polymer the resulting conductive redox polymer can be electrically conducting, have a high charge storage capacity, a well-defined redox potential, and be insoluble in the electrolyte.

We have previously shown that for some polypyrrole/quinone combinations the redox reaction of the quinone severely interferes with the conductivity of the backbone, due to a twisting of the backbone [19]. When poly(3,4-ethylenedioxythiophene) (PEDOT)

* Corresponding author.
E-mail address: martin.sjodin@angstrom.uu.se (M. Sjödin).

https://doi.org/10.1016/j.electacta.2019.03.207

(Fig. 1a) is used as a backbone, this unfavorable polymer-pendant group interaction was not observed [17]. PEDOT, which has been shown to have high conductivity and stability [20], is thus sufficiently robust to withstand forces exerted by the pendant group. In this study we further explore the properties of the quinone-PEDOT conducting redox polymer (Fig. 1b) with the aim to understand the mechanisms involved in charge transfer. We have previously demonstrated a fast redox conversion (sub-second scale) for this material, which tentatively was traced to the material's ability to only cycle protons for charge compensation and the redox matching between the PEDOT backbone and the HQ pendant group [11,17]. The latter condition has been proven to be an absolute requirement for fast redox conversion in conducting redox polymers [11]. In this study we identify the rate-limiting factor in the redox reaction and the charge carrier responsible for conductivity. The former was done by temperature dependent kinetic- and in situ conductance measurements and the latter by electron paramagnetic resonance (EPR) and UV–vis spectroscopy performed in situ during redox conversion. We show that the pendant group redox conversion is rate limited by a thermally activated process that we interpret as the pendant group redox reaction while the electron transport shows non-thermally activated transport properties. We also conclude that bipolarons are formed and show indications that they contribute to the electronic conductivity.

2. Experimental

2.1. General procedures

All solvents and chemicals were purchased from Sigma-Aldrich and were used without further purifications unless otherwise specified. Deionized water was used to prepare aqueous electrolytes and acetonitrile was dried over molecular sieves prior to use. All electrolyte solutions were purged with N_2 prior to measurements and, unless otherwise specified, all experiments were conducted at ambient temperature. EDOT-HQ was synthesized as previously reported [11]. Electrochemical measurements were performed on an Autolab PGSTAT302 N potentiostat (Ecochemie, The Netherlands) equipped with a bipotentiostat module unless otherwise specified. Cyclic voltammetry was used to polymerize the monomer from a 10 mM solution in MeCN, containing 0.1 M $TBAPF_6$ as supporting electrolyte. All characterizations were performed in sulfuric acid (H_2SO_4 (0.5 M), pH 0.3) with a Ag/AgCl (3 M NaCl) (+0.192 V vs. SHE) reference electrode and a platinum wire as counter electrode. All potentials are reported vs. standard hydrogen electrode (SHE) unless otherwise specified. After polymerization the electrodes were rinsed with MeCN and subsequently water before transfer to an H_2SO_4-solution for characterization.

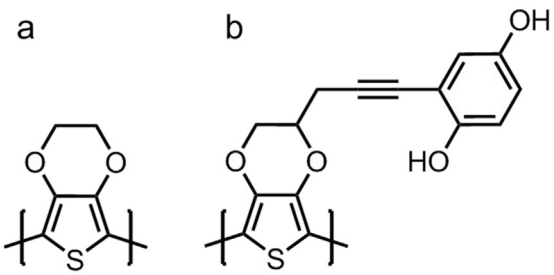

Fig. 1. a) PEDOT and b) PEDOT-HQ.

2.2. In situ conductance

The working electrode for conductance measurements was an interdigitated array (IDA) electrode with 90 pairs of Au bands on glass substrate (10 μm between bands, 150 nm high, MicruX Technologies, Spain). The monomer was polymerized onto the IDA electrode by cyclic voltammetry using three scans between −0.1 V and 1.1 V (vs. $Fc^{0/+}$) at a scan rate of 25 mV/s. The number of scans was chosen as to fully cover the electrode, as verified by visual inspection of the electrode as well as by the constant conductance between second and third cycle monitored during polymerization. Conductance measurements were performed in situ during cyclic voltammetry using a bipotentiostat with a voltage bias between the two working electrodes of 1 mV for polymerization and 10 mV for characterization. A scan rate of 10 mV/s was used for characterization. For the temperature dependence measurements the temperature was increased from 283 K to 343 K in steps of 10 K and the conductance was measured using the same electrode for all temperatures. At the end of the series the temperature was returned to room temperature and the conductance was again measured in order to ensure that the polymer was not degraded during the temperature series.

2.3. Kinetics

A micro glassy carbon (μGC) electrode (BASi) with a diameter of 11 μm was used for the temperature dependence study of the redox reaction of the pendant group. EDOT-HQ was polymerized onto the μGC electrode using two cyclic voltammetry scans between −0.1 V and 1.1 V (vs. $Fc^{0/+}$) at a scan rate of 0.1 V/s. The electrodes were then characterized at temperatures between 283 K and 343 K by cyclic voltammetry while varying the scan rate between 0.1 V/s and 30 V/s at each temperature.

2.4. In situ EPR

For in situ EPR measurements the monomer was polymerized onto a platinum wire (ø = 0.2 mm) working electrode by cyclic voltammetry using five scans between −0.1 V and 1.1 V (vs. $Fc^{0/+}$) at a scan rate of 0.1 V/s. The polymer was then transferred to an electrolytic flat cell (Wilmad LabGlass, USA) filled with 0.5 M H_2SO_4 with the counter and reference electrodes outside the EPR area. EPR spectroscopy was performed with a Bruker EMX-micro spectrometer (Bruker BioSpin, Germany), equipped with an EMX-Premium bridge and an ER4119HS resonator. The microwave frequency was 9.77 GHz, the microwave power was 5 mW, and the modulation amplitude was 1 G. The potential of the polymer was set by potentiostatic methods in steps of 100 mV between 0 V and 1 V, using a CHI660D potentiostat (CH instruments, USA) and was allowed to reach steady state for each potential step before EPR measurements were conducted.

2.5. In situ spectroscopy

The monomer was polymerized onto an indium tin oxide (ITO) coated silicon dioxide glass slide working electrode (Praezisions Glas & Optik GmbH), pre-soaked in potassium acetate [21], by cyclic voltammetry using two scans between −0.1 and 1.3 V (vs. $Fc^{0/+}$) at a scan rate of 0.1 V/s. The polymer was transferred to a 10 × 10 mm quarts cuvette (Quartz SUPRASIL®, Hellma Analytics, Germany) filled with 0.5 M H_2SO_4. The counter and reference electrodes were immersed directly in the cuvette outside of the beam path. An Agilent 8453 UV–visible Spectrophotometer (Agilent Technologies, USA) was used to record the absorption of the polymer during electrochemical redox conversion. Spectra were recorded every

0.5 s during cyclic voltammetry. The polymer was cycled at a scan rate of 10 mV/s in the potential region between 0 V and 1 V. Difference spectra were obtained by subtracting the spectra obtained at 1 V from all other spectra.

3. Results

3.1. Cyclic voltammetry

Fig. 2 shows the voltammetric response from a PEDOT-HQ covered platinum electrode immersed in 0.5 M H_2SO_4 together with the corresponding data for unsubstituted PEDOT. The peak for PEDOT-HQ (black line in Fig. 2) has previously been identified as corresponding to the 2e2H quinone redox conversion [17]. From the cyclic voltammogram (CV) of PEDOT-HQ, the formal potential (E^0) was calculated to 0.67 V, with a peak separation between the oxidation- and reduction peak of 85 mV, an oxidation half peak width of 137 mV and a reduction half peak width of 163 mV at a scan rate of 50 mV/s. At lower scan rates the peak separation is reduced to 50 mV [17].

3.2. In situ conductance

Fig. 3a and c shows the current response from the two working electrodes during electrochemical redox conversion of the polymer. The electrochemical redox conversion is performed by applying a cyclic voltammetry voltage profile on both working electrodes against an external reference and counter electrode while keeping a constant, 10 mV bias, between the two working electrodes. For both PEDOT-HQ and PEDOT the current responses are dominated by the current resulting from the voltage bias between the working electrodes, i.e. the current through the polymer bridging the two working electrodes, which is manifested as a negative current on one electrode and a corresponding positive current on the other electrode. By adding the current responses monitored at the two electrodes, the positive and negative currents originating from current through the polymer cancel out, and the current originating from the redox conversion, i.e. the cyclic voltammetry response, is isolated from the over-all response (Fig. 3b and d for PEDOT-HQ and PEDOT, respectively). The conductance, instead, was calculated by converting the difference between the current responses from the two working electrodes to conductance using ohms law. The current difference corresponds to the current through the material if the conversion currents at the two electrodes are equal or, alternatively, if the current through the material is much larger than the conversion currents thus ensuring that any difference in conversion current at the two electrodes is negligible. As the peaks corresponding to the quinone redox conversion at the two electrodes are close to identical the first condition is met and, in addition, the bias-current dominates the over-all current response (Fig. 3a). In order to avoid double counting of electrons the current difference was divided by two and divided by the voltage bias to yield the polymer conductance (Fig. 3b and d for PEDOT-HQ and PEDOT, respectively).

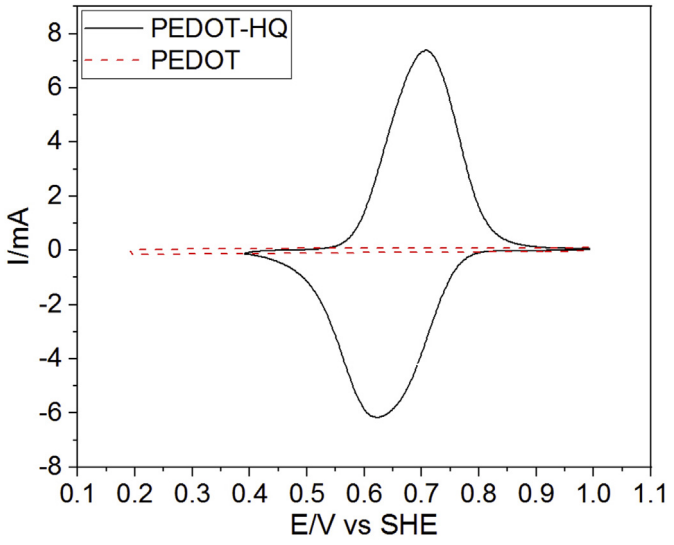

Fig. 2. CV of PEDOT-HQ (black solid line) and PEDOT (red dashed line) on platinum electrodes at a scan rate of 50 mV/s in H_2SO_4 (0.5 M). (For interpretation of the references to colour in this figure legend, the reader is referred to the Web version of this article.)

PEDOT-HQ shows a rapid increase in conductance between −0.1 V and 0.2 V and a close-to-constant conductance plateau around 39 mS at higher potentials (Fig. 3b). PEDOT has a lower onset potential than PEDOT-HQ and could therefore not be brought into an insulating state due to the potential limit of the water electrolytes. PEDOT instead displays an almost constant conductance of 37 mS in the whole potential region investigated.

The conductance was measured at temperatures between 283 K and 343 K for both polymers and the results can be seen in Fig. S2. For PEDOT-HQ, the conductance at 0.67 V was plotted as a function of temperature (Fig. 4) and demonstrates a monotonous decrease with increased temperature, at the formal potential of the quinone. Pristine PEDOT displays a similar behavior (Fig. S2b). For both polymers close to identical in situ conductance response was observed at room temperature after the temperature series as prior to the temperature series.

3.3. Activation energy

For the quinone redox reaction the apparent rate constant was calculated from the slopes at high scan rates in Fig. S1, where the oxidation and reduction peak potentials are plotted against the logarithm of the scan rate. At high scan rates the redox peaks move apart. At sufficiently high scan rates, i.e. when the oxidation or reduction peak has shifted more than 100 mV from E0′, the back reaction was considered negligible and equations for an irreversible forward redox reaction were considered valid. The formal rate constant could then be calculated from the dependence of the peak potential with scan rate using Equation (1) [22].

$$E_p = E^0 \pm \frac{RT}{\alpha z F} \times \ln\left(\frac{\alpha z F \nu}{RTk^0}\right) \quad (1)$$

Here E_p is the peak potential, $E^{0\prime}$ the formal potential, R the gas constant, T the temperature, α the transfer coefficient, z the number of charges, F the faraday constant, ν the scan rate, and k^0 the apparent rate constant.

The apparent rate constant was evaluated at different temperatures (283–343 K) and the results are shown in Fig. 4. The activation energy was obtained using the Arrhenius equation:

$$k = Ae^{-E_a/(RT)} \quad (2)$$

where k is the rate constant, A the Arrhenius constant, E_a the activation energy, R the gas constant, and T the temperature. A fit of the experimental data to Equation (2) (inset Figure) gave an activation energy of 0.30 eV.

3.4. In situ EPR

Fig. 5 shows the EPR signal for PEDOT-HQ and PEDOT measured

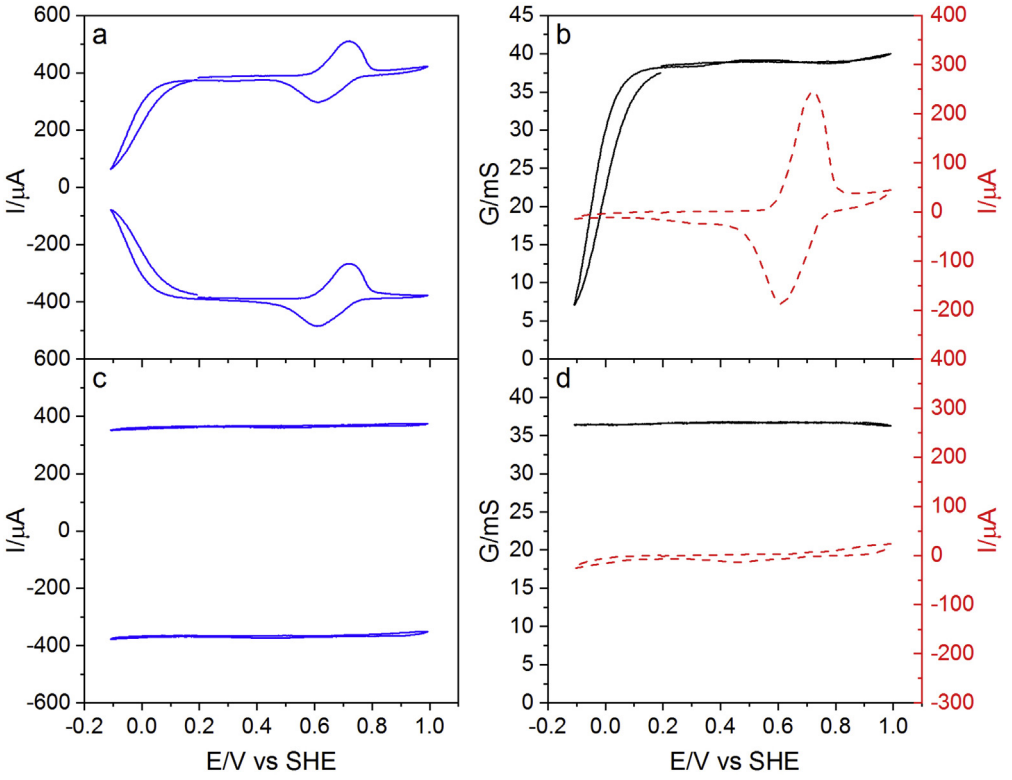

Fig. 3. Individual current responses from the two working electrodes of the IDA electrode for a) PEDOT-HQ and c) PEDOT. The positive and negative currents on the two respective electrodes originate from the current passing through the polymer as a response to the 10 mV bias voltage applied between the electrodes. On top of this bias-current a clear signal originating from the quinone redox conversion is seen in PEDOT-HQ as a response to the cyclic voltammetry excitation against the external reference and counter electrode. The in situ conductance (black solid line) and corresponding CV (red dashed line) were extracted for b) PEDOT-HQ and d) PEDOT from, respectively, the current difference and sum at the two working electrodes. The characterizations were conducted in H_2SO_4 (0.5 M) at a scan rate of 10 mV/s. (For interpretation of the references to colour in this figure legend, the reader is referred to the Web version of this article.)

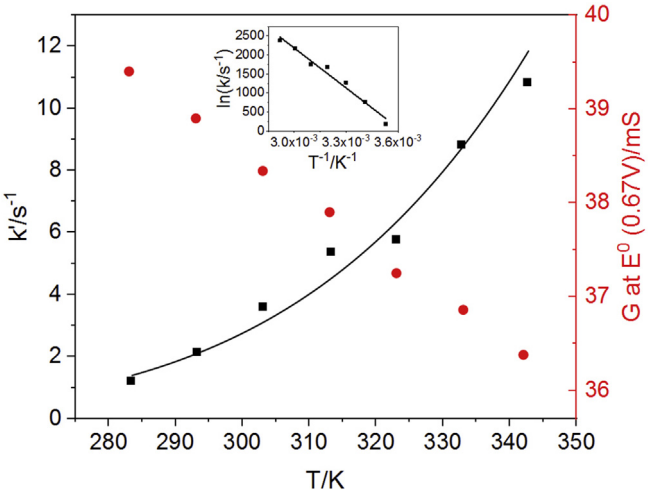

Fig. 4. Temperature dependence of rate constant (black squares) and in situ conductance (red circles) for PEDOT-HQ, showing an activated process for the quinone redox reaction and a non-activated process for the backbone electron transport. A fitting of the rate constants with the Arrhenius equation (inset) gives an activation energy of 0.3 eV. (For interpretation of the references to colour in this figure legend, the reader is referred to the Web version of this article.)

in situ at various potentials. For both polymers all EPR signals show Lorentzian line shapes (Fig. S3) centered around 3486.5 G and 3487.1 G for PEDOT-HQ and PEDOT, respectively. The mean g-value is 2.0026 for both PEDOT-HQ and PEDOT and increases slightly for PEDOT-HQ at higher potentials whereas for PEDOT the g-value does not depend on potential. Relative spin concentrations were calculated by double integration of the derivative signal while the signal width was taken as the distance between the positive and negative peaks.

For PEDOT-HQ the number of spins slightly increases at low potentials, up to 0.3 V, and then starts to decline, see Fig. 6a. PEDOT shows a similar pattern. The signal width increases with potential at low levels of oxidation for both polymers and reaches a plateau around 0.6 V, Fig. 6b.

3.5. *In situ spectroscopy*

From UV–vis differential spectra, Fig. 7, a decrease in the band gap absorbance, accompanied by a small blue-shift, can be seen for both polymers upon oxidation, at ~2.0 eV for PEDOT-HQ and ~2.2 eV for PEDOT. A decrease in the absorption at ~1.4 eV for PEDOT-HQ and ~1.6 eV for PEDOT is also seen upon oxidation. For PEDOT an increase in absorbance is seen at ~1.2 eV. In addition to the PEDOT centered transitions, PEDOT-HQ displays two additional peaks at 3.3 eV and 3.8 eV. The peak at 3.3 eV starts to increase at 0.7 V and the peak at 3.8 eV decreases after 0.7 V, in agreement with the formation of benzoquinone (BQ) (oxidized state) and the disappearance of hydroquinone (HQ) (reduced state), respectively, since the formal potential for the HQ/BQ conversion is at 0.7 V (Figs. 7a and 8).

The band gap absorption of PEDOT-HQ decreases with increased potential and reaches a close-to -constant value after 0.5 V (Fig. 8a). When reducing the polymer the band gap absorption displays

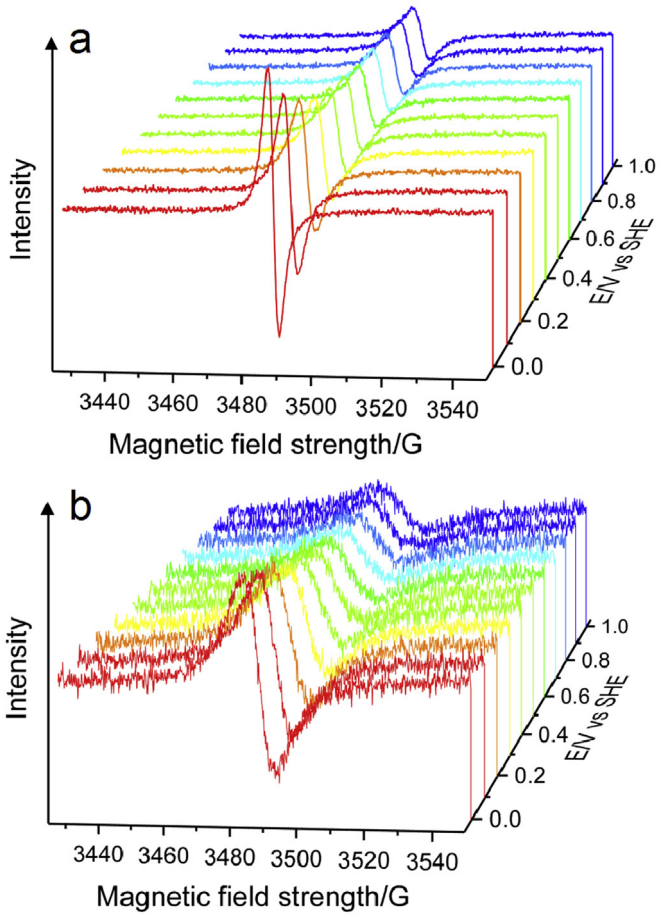

Fig. 5. EPR raw data for a) PEDOT-HQ and b) PEDOT. The characterizations were conducted in H_2SO_4 (0.5 M) while varying potentials were applied to the samples.

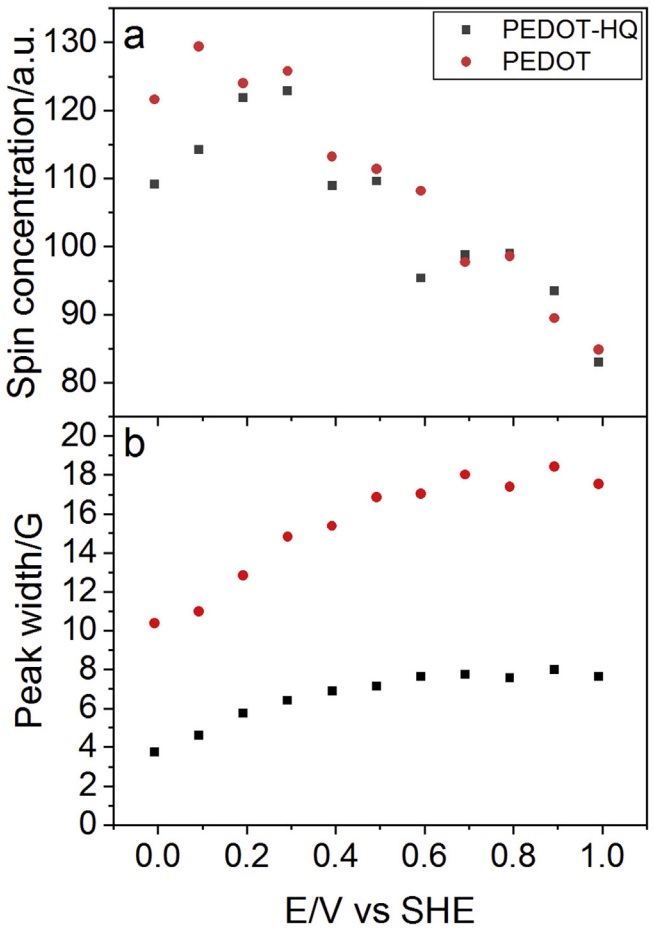

Fig. 6. a) Spin concentration and b) EPR signal width of PEDOT-HQ (black squares) and PEDOT (red circles). (For interpretation of the references to colour in this figure legend, the reader is referred to the Web version of this article.)

complete reversibility (Fig. 8b). The BQ and HQ absorptions also show reversibility with absorption values returning to the original value after a full redox cycle (Fig. 8).

The change in absorbance for BQ and HQ upon oxidation is shown in Fig. 8. The fitted lines are from Equation (4) for BQ (oxidized species) and from Equation (5) for HQ (reduced species), derived from Nernst Equation (3), where x_{ox} (fraction of oxidized species) and x_{red} (fraction of reduced species) are proportional to the absorption:

$$E_{p,ox} = E^{0\prime} + \frac{RT}{zF} \times \ln\left(\frac{C_{ox}}{C_{red}}\right) \tag{3}$$

$$x_{ox} = c_1 \times \frac{e^{(E-E^{0\prime})\times\frac{c_3 zF}{RT}}}{1 + e^{(E-E^{0\prime})\times\frac{c_3 zF}{RT}}} + c_2 \tag{4}$$

$$x_{red} = c_1 \times \frac{1}{1 + e^{(E-E^{0\prime})\times\frac{c_3 zF}{RT}}} + c_2 \tag{5}$$

Here $E^{0\prime}$ is the formal potential, z the number of charges, F the faraday constant, R the gas constant, T the temperature, c_1 the conversion factor to absorption, including the extinction coefficient and polymer thickness, c_2 takes into account the standard error in the baseline, and c_3 is a fudge factor accounting for a deviation from Nernstian behavior.

E^0 was set as a variable and for the green lines, corresponding to a Nernstian fitting, z was set to 2 and c_3 was set to 1 while for the blue lines, corresponding to a non-Nernstian fitting, z was set to 2 and c_3 was set as a variable. The fit yielded a value for c_3 of 0.4 for both HQ and BQ.

4. Discussion

As in all CRPs two redox processes must be considered in PEDOT-HQ, the redox chemistry of the polymer backbone, often referred to as doping, and the redox reaction of the pendant group. In order to benefit from the conducting polymer it is vital for CRPs to have the redox reaction of the pendant group in a potential window where the polymer backbone is conducting, so called redox matching [11]. The condition of redox matching has previously been described for PEDOT-HQ [17] and is also evident from Fig. 3a where the quinone redox reaction, with a formal potential of 0.67 V, is well within the conducting region of the polymer. Furthermore it is desirable that the backbone conductance is relatively unaffected by the redox chemistry of the pendant group, which is not always the case [19]. Also this condition is met in PEDOT-HQ as evidenced by the observation that the quinone redox reaction does not affect the conductivity of the polymer, which shows a constant conductance during the pendant group redox conversion. The fast electron transport through the material could allow for a uniform potential throughout the polymer layer and we can expect the pendant group to be described as a surface-immobilized species. For a fully reversible Nernstian system the

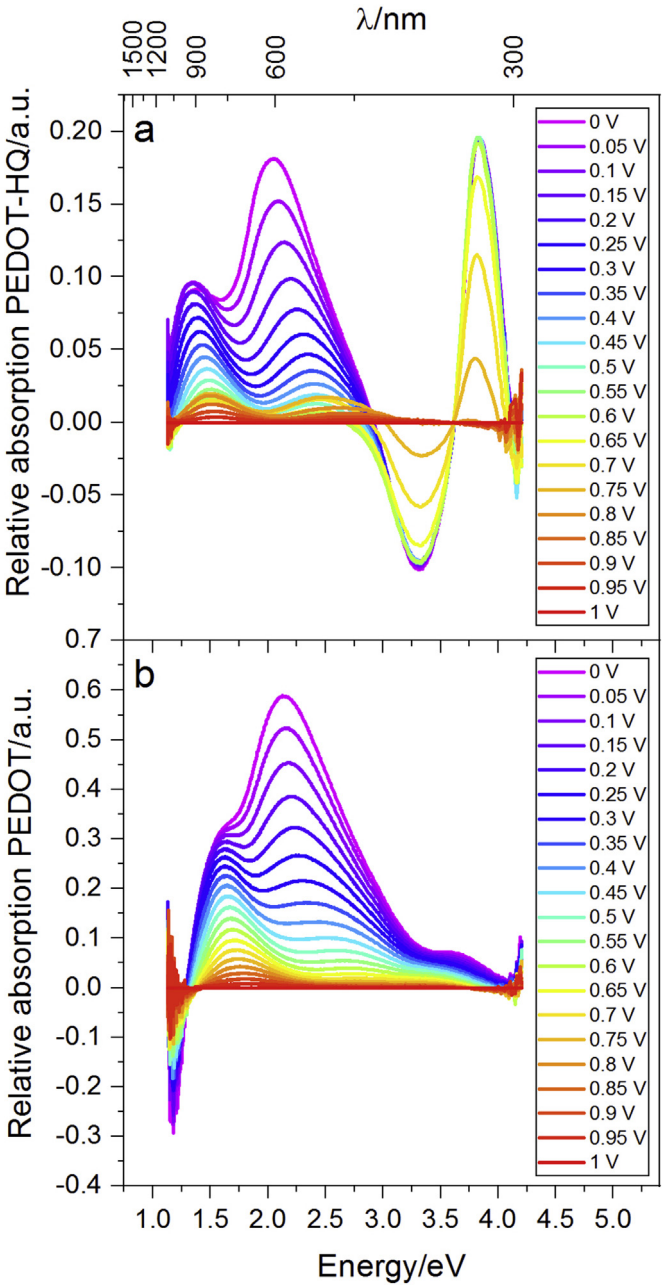

Fig. 7. UV–vis differential spectra of a) PEDOT-HQ and b) PEDOT during oxidation of the polymers in H_2SO_4 (0.5 M). The 1 V spectrum for each polymer is subtracted from the displayed spectra.

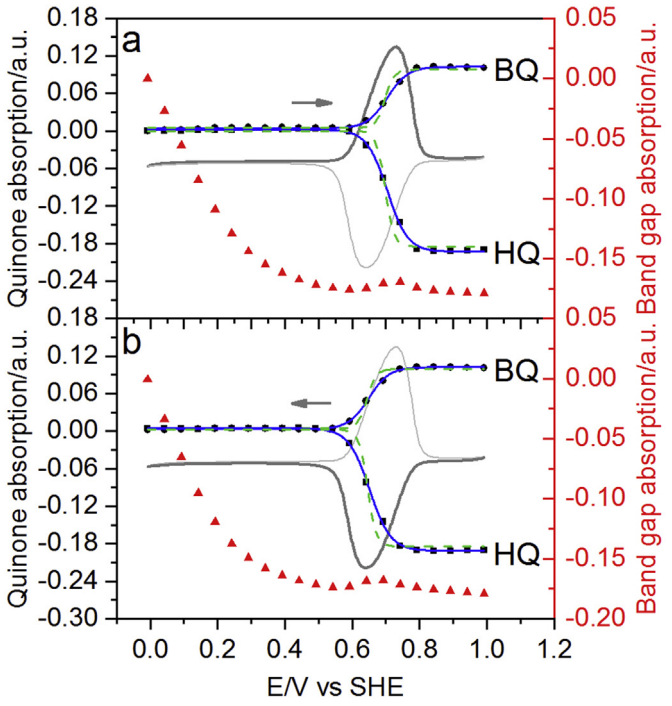

Fig. 8. Absorption values (values from the 0 V spectrum have been subtracted from the displayed values) vs. potential for a) oxidation and b) reduction. BQ values (black circles) are taken at 3.3 eV, HQ values (black squares) are taken at 3.8 eV, and band gap values (red triangles) are taken at 2.1 eV. Green dashed lines correspond to Nernstian fitting and blue solid lines correspond to a non-Nernstian fitting. CVs (grey lines) are added for comparison. (For interpretation of the references to colour in this figure legend, the reader is referred to the Web version of this article.)

peak width should thus be 90.6 mV/n and there should be no peak split [23]. PEDOT-HQ, however, displays a broadened peak as indicated by the half peak width (137 mV) of the redox peaks and a non-zero peak split (85 mV) (Fig. 2). (We have previously shown that the peak split is reduced to 50 mV at lower scan rates [17]). The fittings to Equations (4) and (5), in Fig. 8, of the UV–vis absorption also confirm a deviation from Nernstian behavior with the fudge factor *c3* deviating from 1. The peak broadening indicates interactions between pendant groups. This is expected given the close proximity of redox centers in the polymer as each repeat unit in the polymer carries a quinone substituent [24–26]. The pendant groups have the possibility for π-π-interactions in both reduced and oxidized states, and hydrogen bonding between hydroxy groups in the reduced state with either other hydroxy groups or carbonyl groups in the oxidized state.

The electron transport through the polymer can be facilitated by a temperature increase as the additional thermal energy available may overcome activation barriers involved in the electron transport. This thermally assisted electron transport results in a positive temperature dependence as observed for several conducting polymer systems [27–32]. But when the temperature is increased, thermally activated phonons are also introduced into the polymer and will result in an increased scattering of charge carriers [33,34], and thus a lowered conductivity. PEDOT-HQ and PEDOT display a negative dependence of the conductance with increased temperature (Fig. S2) and hence the activation barrier is sufficiently low so that an increased scattering dominates the temperature dependence in the studied temperature interval (283–343 K). Although a negative temperature dependence of the conductance has previously been reported [35] what we present here is, to the best of our knowledge, the first time a negative temperature dependence is reported for a CRP in the potential region where the pendant group redox reaction occurs.

EPR results (Fig. 6a) show a polaron concentration that is lowered at higher potential, and equivalently at higher doping level. Both PEDOT-HQ and PEDOT show similar changes in spin concentration, indicating no big difference in polaron formation and depletion between the two polymers. The peaks in the UV–vis spectra (Fig. 7) at low energy, ~1.3 eV for PEDOT-HQ and ~1.6 eV for PEDOT, follow the same trend as the EPR results and can be assigned to polarons. The decrease in spin concentration has been observed previously and is generally interpreted as the formation of spinless bipolarons [36–39]. The decreased spin concentration at higher potentials is, however, not concomitant with a decreased

conductance, i.e. the conductance remains at a constant plateau value. The constant conductance can be interpreted in two ways: either the bipolarons formed at high doping level contribute to the conductivity or the formation of bipolarons increases the mobility for the remaining polarons. An increase in EPR signal width (Fig. 6b) indicates that the spin is changing, which could be due to a different environment around the polarons upon doping which has, for spins with Lorentzian line-shapes, been connected to a decrease in mobility [40]. This gives support to the claim that the bipolarons are indeed also charge carriers.

The apparent rate constant for quinone redox conversion evaluated at E^0 follows an Arrhenius behavior, indicating a thermally activated rate-limiting reaction in the redox conversion process with an activation energy of 0.3 eV (Fig. 4). This is in clear contrast to the non-thermally activated behavior found for electron transport trough the polymer, as evaluated from the polymer conductance measurements under steady-state conditions at the same potential (Fig. 4). We can thus conclude that electron transport through the polymer does not limit the quinone redox conversion rate. From investigating the cyclic voltammetry response at different scan rates we have previously also shown that the redox reaction is not diffusion limited [17].

As the electron transport is fast relative to the quinone redox conversion we can assume that the polymer backbone is in equilibrium with the electrode on the time-scale of quinone redox conversion and hence that at E^0, where the apparent rate constant is evaluated, the polymer backbone is equilibrated. The oxidation reaction going from HQ to BQ is complex and contains four elementary reactions, two electron transfer steps and two deprotonation steps, and a minimum of five different states and the route to BQ can follow several different routes, see Scheme 1. Identifying the reaction sequence which gives rise to the apparent activation energy of 0.3 eV is thus difficult. However, the fully protonated fully oxidized state (H_2Q^{2+}) and the fully deprotonated fully reduced state (Q^{2-}) are not probable since they are located at too high energies. For the HQ^- state to be formed H_2Q would have to be deprotonated. However, we see no indication of a deviation from the −59 meV/pH slope of the quinone formal potential up to at least pH 13 suggesting that the HQ does not deprotonate below pH 13. Initial deprotonation of the hydroquinone is thus highly endergonic with an energy barrier of more than 750 meV that has to be overcome in order for the reaction to occur. Since the observed activation energy is significantly below this barrier the HQ^- intermediate is unlikely. The first step in the oxidation sequence must instead be the electron transfer from H_2Q to the polymer backbone forming H_2SQ^+, followed by deprotonation of the semiquinone radical to form the neutral HSQ. As only one peak, corresponding to the complete conversion from HQ to BQ, is seen in the CV at any scan rate [17] we can further conclude that the semiquinone state is not only unstable with respect to disproportionation but its formation step is slower than the subsequent reaction leading to the fully oxidized state regardless of which route is taken. Consequently, the rate determining steps will be the electron transfer from H_2Q forming H_2SQ^+, the deprotonation of H_2SQ^+ to form HSQ, or a combination of both and the activation energy determined is associated with this reaction sequence. With a rate-limiting electron transfer step, the activation energy is simply the activation barrier for the electron transfer between H_2Q to PEDOT. With a rate-limiting deprotonation, the activation barrier is instead given by the activation energy for the deprotonation reaction and the temperature dependence of the equilibrium between H_2Q and H_2SQ^+. We cannot, at present, differentiate between these limiting cases. Regardless of which reaction is limiting we can conclude that it is one of these elementary steps and not the electron transport through the polymer, since that would result in the same negative temperature dependence for the quinone redox reaction as for the conductance.

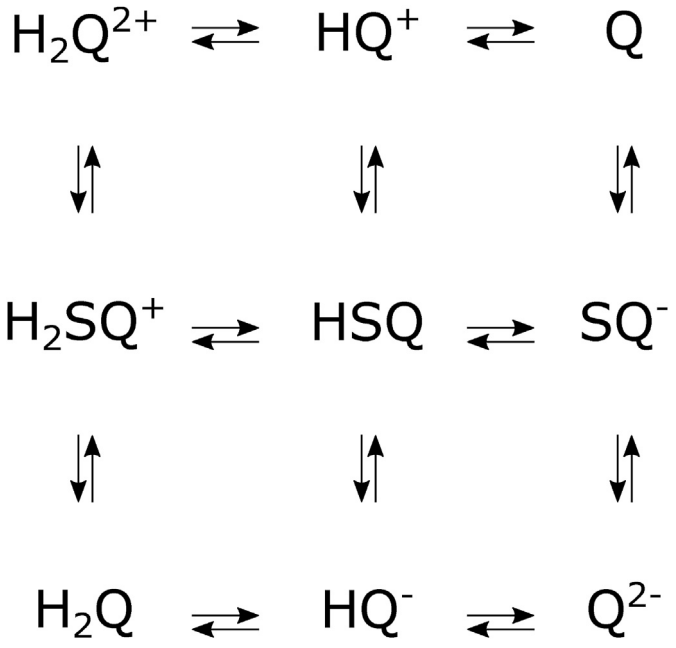

Scheme 1. Square scheme of the redox processes involved in the conversion between hydroquinone and benzoquinone, in this graph denoted H_2Q and Q, respectively. SQ stands for semiquinone. Electronic transitions are represented with vertical arrows and proton transfers are represented with horizontal arrows.

5. Conclusion

The redox reaction of PEDOT-HQ in an acidic electrolyte was studied by various in situ methods. The redox conversion of PEDOT-HQ deviates from Nernst behavior with a broadened peak and a peak split between the oxidation and reduction peaks as well as a fitting to the in situ UV–vis absorbance that does not follow Nernstian behavior. The HQ/BQ redox conversion exhibits a thermally activated process with an activation energy, for the rate-limiting step, of 0.3 eV while the electron transport through the polymer is a non-thermally activated process. The electron transport is thus not rate-limiting and the redox reaction is instead limited by a proton or electron transfer to or from the quinone pendant group. We have hence narrowed down which steps in the redox process that could be rate determining. This is the first time a negative temperature dependence has been presented for a conducting redox polymer in the potential region where the redox active pendant group has its formal potential. In situ EPR and in situ conductance data indicates that bipolarons are charge carriers since the polaron concentration decreases and the polarons become less mobile while the conductance is constant. These results give us a clearer picture of how charges move in the CRP and which steps in the redox conversion should be focused on in order to improve the reaction rate.

Acknowledgements

This work was founded by, the Carl Trygger Foundation, the Swedish Energy Agency, the Swedish Research Council (VR), the Olle Engqvist Byggmästare Foundation and The Research Council Formas.

Appendix A. Supplementary data

Supplementary data to this article can be found online at https://doi.org/10.1016/j.electacta.2019.03.207.

References

[1] M. Armand, J.-M. Tarascon, Building better batteries, Nature 451 (2008) 652–657.
[2] L.A.-W. Ellingsen, G. Majeau-Bettez, B. Singh, A.K. Srivastava, L.O. Valøen, A.H. Strømman, Life cycle assessment of a lithium-ion battery vehicle pack, J. Ind. Ecol. 18 (2014) 113–124.
[3] X.-Q. Zhu, C.-H. Wang, Accurate estimation of the one-electron reduction potentials of various substituted quinones in DMSO and CH3CN, J. Org. Chem. 75 (2010) 5037–5047.
[4] B. Häupler, A. Wild, U.S. Schubert, Carbonyls: powerful organic materials for secondary batteries, Adv. Energy Mater. 5 (2015) 1402034.
[5] C. Karlsson, T. Suga, H. Nishide, Quantifying TEMPO redox polymer charge transport toward the organic radical battery, ACS Appl. Mater. Interfaces 9 (2017) 10692–10698.
[6] T. Janoschka, M.D. Hager, U.S. Schubert, Powering up the future: radical polymers for battery applications, Adv. Mater. 24 (2012) 6397–6409.
[7] W. Luo, M. Allen, V. Raju, X. Ji, An organic pigment as a high-performance cathode for sodium-ion batteries, Adv. Energy Mater. 4 (2014) 1400554.
[8] W. Huang, Z. Zhu, L. Wang, S. Wang, H. Li, Z. Tao, J. Shi, L. Guan, J. Chen, Quasi-solid-state rechargeable lithium-ion batteries with a calix[4]quinone cathode and gel polymer electrolyte, Angew. Chem. Int. Ed. 52 (2013) 9162–9166.
[9] P. Novák, K. Müller, K.S.V. Santhanam, O. Haas, Electrochemically active polymers for rechargeable batteries, Chem. Rev. 97 (1997) 207–282.
[10] K. Gurunathan, D.P. Amalnerkar, D.C. Trivedi, Synthesis and characterization of conducting polymer composite (PAn/TiO2) for cathode material in rechargeable battery, Mater. Lett. 57 (2003) 1642–1648.
[11] R. Emanuelsson, M. Sterby, M. Strømme, M. Sjödin, An all-organic proton battery, J. Am. Chem. Soc. 139 (2017) 4828–4834.
[12] K. Nueangnoraj, T. Tomai, H. Nishihara, T. Kyotani, I. Honma, An organic proton battery employing two redox-active quinones trapped within the nanochannels of zeolite-templated carbon, Carbon 107 (2016) 831–836.
[13] H. Chen, M. Armand, G. Demailly, F. Dolhem, P. Poizot, J.-M. Tarascon, From biomass to a renewable LiXC6O6 organic electrode for sustainable Li-ion batteries, ChemSusChem 1 (2008) 348–355.
[14] Y. Liang, Z. Tao, J. Chen, Organic electrode materials for rechargeable lithium batteries, Adv. Energy Mater. 2 (2012) 742–769.
[15] S. Renault, V.A. Mihali, K. Edström, D. Brandell, Stability of organic Na-ion battery electrode materials: the case of disodium pyromellitic diimidate, Electrochem. Commun. 45 (2014) 52–55.
[16] C. Karlsson, H. Huang, M. Strømme, A. Gogoll, M. Sjödin, Ion- and electron transport in pyrrole/quinone conducting redox polymers investigated by in situ conductivity methods, Electrochim. Acta 179 (2015) 336–342.
[17] M. Sterby, R. Emanuelsson, X. Huang, A. Gogoll, M. Strømme, M. Sjödin, Characterization of PEDOT-quinone conducting redox polymers for water based secondary batteries, Electrochim. Acta 235 (2017) 356–364.
[18] L. Åkerlund, R. Emanuelsson, S. Renault, H. Huang, D. Brandell, M. Strømme, M. Sjödin, The proton trap technology—toward high potential quinone-based organic energy storage, Adv. Energy Mater. 7 (2017) 1700259.
[19] C. Karlsson, H. Huang, M. Strømme, A. Gogoll, M. Sjödin, Ion- and electron transport in pyrrole/quinone conducting redox polymers investigated by in situ conductivity methods, Electrochim. Acta 179 (2015) 336–342.
[20] A. Elschner, PEDOT: Principles and Applications of an Intrinsically Conductive Polymer, CRC Press, Boca Raton, 2011.
[21] C. Karlsson, H. Huang, M. Strømme, A. Gogoll, M. Sjödin, Polymer–pendant interactions in poly(pyrrol-3-ylhydroquinone): a solution for the use of conducting polymers at stable conditions, J. Phys. Chem. C 117 (2013) 23558–23567.
[22] E. Laviron, General expression of the linear potential sweep voltammogram in the case of diffusionless electrochemical systems, J. Electroanal. Chem. Interfacial Electrochem. 101 (1979) 19–28.
[23] A.J. Bard, L.R. Faulkner, Electrochemical Methods: Fundamentals and Applications, second ed., John Wiley & Sons, New York, NY, 2001.
[24] J.A. Tossell, Quinone–hydroquinone complexes as model components of humic acids: theoretical studies of their structure, stability and Visible–UV spectra, Geochim. Cosmochim. Acta 73 (2009) 2023–2033.
[25] B.G. Bravo, T. Mebrahtu, M.P. Soriaga, D.C. Zapien, A.T. Hubbard, J.L. Stickney, Reversible redox of 2,5-dihydroxythiophenol chemisorbed on gold and platinum electrodes: evidence for substrate-mediated adsorbate-adsorbate interactions, Langmuir 3 (1987) 595–597.
[26] M.P. Soriaga, A.T. Hubbard, Electrode reactions of oriented chemisorbed molecules: the effect of temperature on reversible redox, irreversible oxidation, and reductive desulfurization, J. Electroanal. Chem. Interfacial Electrochem. 159 (1983) 101–116.
[27] H. Huang, C. Karlsson, F. Mamedov, M. Strømme, A. Gogoll, M. Sjödin, Polaron disproportionation charge transport in a conducting redox polymer, J. Phys. Chem. C 121 (2017) 13078–13083.
[28] C. Oh Yoon, J. Hyun Kim, H. Kyung Sung, J. Hun Kim, K. Lee, H. Lee, Transport studies of emeraldine salts protonated by phosphoric acids, Synth. Met. 81 (1996) 75–80.
[29] N.T. Kemp, A.B. Kaiser, C.-J. Liu, B. Chapman, O. Mercier, A.M. Carr, H.J. Trodahl, R.G. Buckley, A.C. Partridge, J.Y. Lee, C.Y. Kim, A. Bartl, L. Dunsch, W.T. Smith, J.S. Shapiro, Thermoelectric power and conductivity of different types of polypyrrole, J. Polym. Sci., Part B: Polym. Phys. 37 (1999) 953–960.
[30] W. Liu, N. Liu, J. Sun, P.-C. Hsu, Y. Li, H.-W. Lee, Y. Cui, Ionic conductivity enhancement of polymer electrolytes with ceramic nanowire fillers, Nano Lett. 15 (2015) 2740–2745.
[31] K. Wilbourn, R.W. Murray, The d.c. redox versus electronic conductivity of the ladder polymer poly(benzimidazobenzophenanthroline), J. Phys. Chem. 92 (1988) 3642–3648.
[32] S. Wang, H. Sun, U. Ail, M. Vagin, P.O.Å. Persson, J.W. Andreasen, W. Thiel, M. Berggren, X. Crispin, D. Fazzi, S. Fabiano, Thermoelectric properties of solution-processed n-doped ladder-type conducting polymers, Adv. Mater. 28 (2016) 10764–10771.
[33] T.M. Swager, , 50th anniversary perspective: conducting/semiconducting conjugated polymers. A personal perspective on the past and the future, Macromolecules 50 (2017) 4867–4886.
[34] O. Bubnova, Z.U. Khan, H. Wang, S. Braun, D.R. Evans, M. Fabretto, P. Hojati-Talemi, D. Dagnelund, J.-B. Arlin, Y.H. Geerts, S. Desbief, D.W. Breiby, J.W. Andreasen, R. Lazzaroni, W.M. Chen, I. Zozoulenko, M. Fahlman, P.J. Murphy, M. Berggren, X. Crispin, Semi-metallic polymers, Nat. Mater. 13 (2013) 190.
[35] L. Yang, X. Huang, F. Mamedov, P. Zhang, A. Gogoll, M. Strømme, M. Sjödin, Conducting redox polymers with non-activated charge transport properties, Phys. Chem. Chem. Phys. 19 (2017) 25052–25058.
[36] W. Domagala, B. Pilawa, M. Lapkowski, Quantitative in-situ EPR spectroelectrochemical studies of doping processes in poly(3,4-alkylenedioxythiophene) s: Part 1: PEDOT, Electrochim, Acta 53 (2008) 4580–4590.
[37] G. Zotti, S. Zecchin, G. Schiavon, L.B. Groenendaal, Conductive and magnetic properties of 3,4-dimethoxy- and 3,4-ethylenedioxy-capped polypyrrole and polythiophene, Chem. Mater. 12 (2000) 2996–3005.
[38] P. Rapta, A. Neudeck, A. Petr, L. Dunsch, In situ EPR/UV–VIS spectroelectrochemistry of polypyrrole redox cycling, J. Chem. Soc., Faraday Trans. 94 (1998) 3625–3630.
[39] A.V. Volkov, S.K. Singh, E. Stavrinidou, R. Gabrielsson, J.F. Franco-Gonzalez, A. Cruce, W.M. Chen, D.T. Simon, M. Berggren, I.V. Zozoulenko, Spectroelectrochemistry and nature of charge carriers in self-doped conducting polymer, Adv. Electronic Mater. 3 (2017) 1700096.
[40] M. Schärli, H. Kiess, G. Harbeke, W. Berlinger, K.W. Blazey, K.A. Müller, E.S.R. of BF4−-doped polythiophene, Synth. Met. 22 (1988) 317–336.